EEET ECOLOGICAL ENGINEERING & ENVIRONMENTAL TECHNOLOGY

Ecological Engineering & Environmental Technology 2024, 25(10), 297–305
https://doi.org/10.12912/27197050/191989
ISSN 2299–8993, License CC-BY 4.0

Received: 2024.07.07
Accepted: 2024.08.15
Published: 2024.09.01

Simple Preparation of Iron Oxide-Loaded Biochar from *Ceratophyllum demersum* for Fenton-Like Degradation of Rhodamine B

Phong Thanh Tran[1,2], Hung Minh Nguyen[1,2], Khang Dinh Vo[1,2], Long Quang Nguyen[1,2], Tuyet-Mai Tran-Thuy[1,2], Dung Van Nguyen[1,2*]

[1] Faculty of Chemical Engineering, Ho Chi Minh City University of Technology (HCMUT), 268 Ly Thuong Kiet Street, District 10, Ho Chi Minh City, Vietnam

[2] Vietnam National University Ho Chi Minh City, Linh Trung Ward, Thu Duc City, Ho Chi Minh City, Vietnam

* Corresponding author's e-mail: nvdung@hcmut.edu.vn

ABSTRACT

The current study aims to valorize *C. demersum*, a common aquatic plant in lakes, ponds, and quiet streams with little use. $FeCl_3$-impregnated *C. demersum* was directly pyrolyzed to yield iron oxide-loaded biochar (IO/BC). Analytical results revealed that 3.19 wt% Fe existed in the resulting composite, including predominant hematite (α-Fe_2O_3) and minor magnetite (Fe_3O_4). Moreover, the total pore volume (V_{total}) and the specific surface area (S_{BET}) of IO/BC were 0.091 cm^3/g and 113 m^2/g, respectively. IO/BC was subsequently explored for catalytic rhodamine B (RhB) degradation using H_2O_2. At pH 3.0, 30 °C, 1.00 g/L IO/BC partly eliminated 18% RhB (20 ppm), corresponding to an adsorption capacity of 3.6 mg/g. Upon the addition of 120 ppm H_2O_2, total RhB removal reached 92% after 90 min. Furthermore, RhB treatment was consistent with the pseudo-first-order kinetics. The rate constant (k) at 30 °C was 0.0260 min^{-1}, and the activation energy (E_a) was 72 kJ/mol. Overall, the findings highlighted the catalytic potential of IO/BC prepared from *C. demersum* for Fenton-like degradation of RhB.

Keywords: *Ceratophyllum demersum*, biomass valorization, iron oxide, biochar, Fenton-like process, rhodamine B.

INTRODUCTION

Nowadays, various human activities and industrial processes release considerable quantities of diverse organic pollutants, notably pharmaceuticals, pesticides, and dyes, into water environments (Chen et al., 2023; Lu and Astruc, 2020). These pollutants can poison aquatic organisms, reduce biodiversity, and pose health risks to humans (Mukhopadhyay et al., 2022; Titchou et al., 2021). Although some pollutants degrade rapidly, others endure and accumulate in the food chain, necessitating effective remediation efforts (Filote et al., 2021). For that purpose, Fenton and Fenton-like reactions are widely used, thanks to their high efficiency, simplicity, and ability to operate under ambient conditions (Liu and Wang, 2023; Novia et al., 2023). These processes convert eco-friendly and cost-effective but low-reactive hydrogen peroxide (H_2O_2) into highly reactive hydroxyl radicals (•OH) for degrading organic contaminants (Shokri and Fard, 2022). The Fenton reaction utilizes Fe^{2+} ions, whereas Fenton-like processes involve the use of Fe^{3+} or other metal ions (Wang et al., 2016). To minimize sludge formation, solid catalysts have been interested (Nguyen et al., 2024). Iron oxides like magnetite (Fe_3O_4), hematite (α-Fe_2O_3), and maghemite (γ-Fe_2O_3) are preferred for Fenton and Fenton-like processes due to their effective hydroxyl radical generation, stability, reusability, cost-effectiveness, and environmental compatibility (Pouran et al., 2014; Zhu et al., 2019). However, iron oxide particles have the tendency to form agglomerates during their use (Gutiérrez et al., 2019). This phenomenon can affect their catalytic activity and overall efficiency (Rusevova et al., 2012). To prevent agglomeration, iron oxide particles can be immobilized onto proper supports.

Biochar (BC) is a carbon-based material produced from biomass pyrolysis in oxygen-limited conditions (Gupta et al., 2022; Qin et al., 2022). It has garnered significant interest as a support for metal oxides in various applications, particularly in environmental remediation (Weidner et al., 2022; Zhao et al., 2021). The porous structure of BC provides ample space for the uniform distribution of metal oxides, enhancing their reactivity and stability (Pereira Lopes and Astruc, 2021). Compared with activated carbon and other supports, BC is inexpensive, making it an economically viable option for large-scale applications (Masud et al., 2023). To facilely load iron oxides within BC, direct pyrolysis of $FeCl_3$-impregnated biomass has been applied in recent years (Qu et al., 2022; Yi et al., 2020). Based on pyrolysis conditions, $FeCl_3$ can be converted into Fe_2O_3, Fe_3O_4, and even Fe (Bedia et al., 2020; Nguyen et al., 2023). These iron-based particles can be immobilized within the BC structure, enhancing the stability and reusability of the resulting IO/BC composite (Feng et al., 2021). Furthermore, $FeCl_3$ can play an activation role to improve porous properties of BC support (Bedia et al., 2020; Zeng and Kan, 2022). Owing to these advantages, the above-mentioned approach was used to fabricate IO/BC from biomass.

According to Do et al. (2022), biomass resources have significant influences on different properties and catalytic performance of IO/BC products. More importantly, the investigation of untapped biomass resources could provide additional scientific knowledge for the expanded selection of proper IO/BCs in later research and industrial uses. Hence, unnoticed *C. demersum* was selected for investigation in this study. This species, also referred to as coontail or hornwort, is a submerged, free-floating aquatic plant (Polechońska et al., 2018). *C. demersum* is a global species that is found in slow-moving streams, marshes, ditches, lakes, and ponds in both temperate and tropical regions (Keskinkan et al., 2004). It features thin, dark green to blackish stems with whorls of finely divided leaves (Qadri et al., 2022). In regards to its ecological role, *C. demersum* provides habitat and oxygenation for aquatic life, competes with algae, and offers cover for fish and invertebrates (Wang et al., 2023). This plant also acts as a biofilter, enhancing water quality. Although *C. demersum* is popular in aquariums and garden ponds for its aesthetic appeal and water-clarifying properties, this demand is minimal. According to Mokrzycki et al. (2021), *C. demersum* can be considered an aggressive aquatic weed because of its rapid growth. Consequently, the abundant, available, and underutilized *C. demersum* becomes a promising biomass resource for the preparation of IO/BC. The as-prepared material was accordingly explored as a potential Fenton-like catalyst to eliminate RhB, a synthetic dye widely used in a variety of industries (Ghibate et al., 2024).

EXPERIMENTAL

Raw material and chemicals

Fresh *C. demersum* was gathered from a ditch in Can Tho province, Vietnam. The biomass was initially cleaned with fresh water and then with tap water to effectively remove almost all dust and soil. *C. demersum* was dried at 105 °C for 24 h in a laboratory oven before being crushed into a fine powder by an electric grinder. The biomass was then stored in a closed jar for further use. $FeCl_3 \cdot 6H_2O$ (≥ 99.0%), HNO_3 (65.0~68.0%), H_2SO_4 (95.0~98.0%), NaOH (≥ 96.0%), $Na_2HPO_4 \cdot 12H_2O$ (≥ 99.0%), and H_2O_2 (≥ 30.0%) were bought from Xilong Scientific Co., Ltd. KH_2PO_4 (≥ 99.5%), and $Na_2S_2O_3 \cdot 5H_2O$ (≥ 99.0%) were received from Guangdong Guanghua Sci-Tech Co., Ltd. Rhodamine B was obtained from Shanghai Zhanyun Chemical Co., Ltd.

Preparation of IO/BC

The methodology for preparing IO/BC from *C. demersum* was modified from previous studies on other biomass resources (Do et al., 2022; Nguyen et al., 2023). First, 4.00 g of *C. demersum* powder was added to 100 mL of a solution containing 0.80 g of $FeCl_3$ in a 200 mL beaker. The mixture was magnetically stirred for 15 h and dried at 105 °C for 24 h in the aforementioned oven. Subsequently, $FeCl_3$-impregnated *C. demersum* was put in a vertical tubular reactor, which flowed continuously with nitrogen gas (250 mL/min). An electric oven was used to increase the temperature of the reactor from room temperature with a heating rate of 5 °C/min. Pyrolysis was then conducted at 600 °C for 60 min. The obtained solid was rinsed meticulously with distilled water and subjected to drying at 80 °C for 24 h in a laboratory oven, creating IO/BC. In the same procedure, BC was prepared from *C. demersum* without $FeCl_3$ impregnation.

Characterization of IO/BC

Crystalline structures of BC and IO/BC were determined by X-ray diffraction (XRD) using a D2 phaser diffractometer (Cu-Kα radiation) over a 2θ range of 5–80°. To analyze the Fe content in IO/BC, the material was first immersed in concentrated HNO_3 at 50 °C for 1 h. The obtained solution was then quantified by a Perkin Elmer Optima 7300 DV ICP-OES system. Nitrogen adsorption and desorption isotherms of BC and IO/BC were studied by a surface area and pore size analyzer (Quantachrome Nova 4000e) at 77 K. Two samples were outgassed at 300 °C for 5 h. S_{BET} was determined using the BET Equation, whereas V_{total} was calculated at P/P_o of 0.99. Lastly, scanning electron microscopy (SEM) images of IO/BC were obtained from a JEOL JSM-IT200 instrument.

Fenton-like degradation of RhB catalyzed by IO/BC

The catalytic performances of BC and IO/BC were assessed via RhB degradation using H_2O_2. The experimental procedure was referenced from prior research (Nguyen et al., 2021). The treatment included two steps: adsorption and oxidation. First, a certain catalyst dosage was introduced to 100 mL of RhB solution (20 ppm) in a 200 mL beaker. The mixture was mechanically stirred during the treatment. For specific temperatures, heating and cooling apparatuses were used. The initial pH was changed by 0.1 M H_2SO_4 and 0.1 M NaOH solutions. After 30 min of adsorption, a certain H_2O_2 dosage was swiftly added to the mixture for the oxidation step. Withdrawn samples were promptly added to solutions containing both phosphate buffer and $Na_2S_2O_3$. The catalysts were removed by centrifugation, and the remaining RhB concentrations were measured by a spectrophotometer at 553 nm. For the adsorption step, RhB removal (%) and adsorption capacity (mg/g) were computed by the following Equations:

$$\text{Adsorption capacity (mg/g)} = \frac{20 - C_0}{C_A} \quad (1)$$

$$\text{RhB removal (\%)} = \frac{20 - C_0}{20} \times 100\% \quad (2)$$

where: C_A (g/L) was labeled for BC or IO/BC dosages. The initial RhB concentration was 20 ppm, whereas C_0 (ppm) was the RhB concentration after 30 min of adsorption.

For the oxidation step, total RhB removal was calculated as follows:

$$\text{Total RhB removal (\%)} = \frac{20 - C_{90}}{20} \times 100\% \quad (3)$$

where: C_{90} (ppm) was the remaining RhB concentration after 90 min of oxidation.

RESULTS AND DISCUSSION

Properties of IO/BC

XRD patterns of BC and IO/BC are presented in Figure 1. In both materials, highly noisy baselines are observed, possibly due to the amorphous phases of BC and iron-based components. Notably, BC from *C. demersum* contains peaks of quartz crystals (SiO_2). Naturally, *C. demersum* is an aquatic plant that could absorb minerals from soil and water. Compared with BC, IO/BC contained peaks of not only quartz but also α-Fe_2O_3 and Fe_3O_4. As indicated by the difference in the height of the main peaks, α-Fe_2O_3 was the major Fe-based product, while Fe_3O_4 was the minor one. In addition, quantitative analysis revealed that 3.19 wt% Fe was present within IO/BC (Table 1). Based on prior studies (Bedia et al., 2020; Nguyen et al., 2023), the formation route of these oxides is suggested as follows:

$$C.demersum \rightarrow C, CO_2, H_2O \quad (4)$$

$$FeCl_3 \xrightarrow{+H_2O} FeOOH \rightarrow \rightarrow Fe_2O_3 \xrightarrow{+C} Fe_3O_4 \xrightarrow{+C} Fe \quad (5)$$

During pyrolysis, the biomass could be decomposed into carbon, steam, and other gases. Then, $FeCl_3$ could be hydrolyzed to create

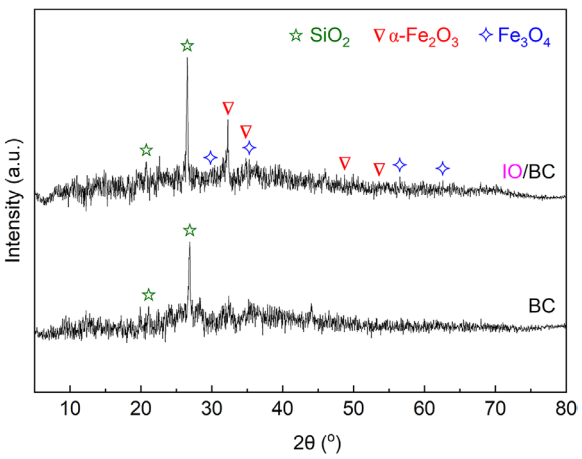

Figure 1. XRD patterns of BC and IO/BC

α-Fe_2O_3 as the main iron-based component in IO/BC. Due to the limit on H_2O release, only a portion of $FeCl_3$ could be converted. The remaining $FeCl_3$ was removed during the cleaning step. Under the existence of carbon and other potential reducing agents, a certain part of α-Fe_2O_3 could be converted into Fe_3O_4.

The porous properties of BC and IO/BC were studied by nitrogen adsorption and desorption (Figure 2). For both samples, the adsorbed volumes gradually increased when P/P_o augmented from 0.009 to 0.99. These results demonstrated that BC and IO/BC contained wide ranges of pore sizes. These findings are further illustrated by BJH pore size distributions. BC had a typical pore size of 1.9 nm, while that of IO/BC was 3.5 nm. As provided in Table 1, BC only possessed a V_{total} of 0.042 cm^3/g and a S_{BET} of 21 m^2/g. With $FeCl_3$ addition, V_{total} and S_{BET} of IO/BC were enhanced to 0.091 cm^3/g and 113 m^2/g, respectively. Undoubtedly, $FeCl_3$ could activate the porous system of BC (Bedia et al., 2020). Although iron oxide particles may obstruct certain pores, newly created pores or extended existing pores through activation might be superior.

Table 1. Properties of BC and IO/BC

Material	Fe (wt%)	S_{BET} (m^2/g)	V_{total} (cm^3/g)
BC	–	21	0.042
IO/BC	3.19	113	0.091

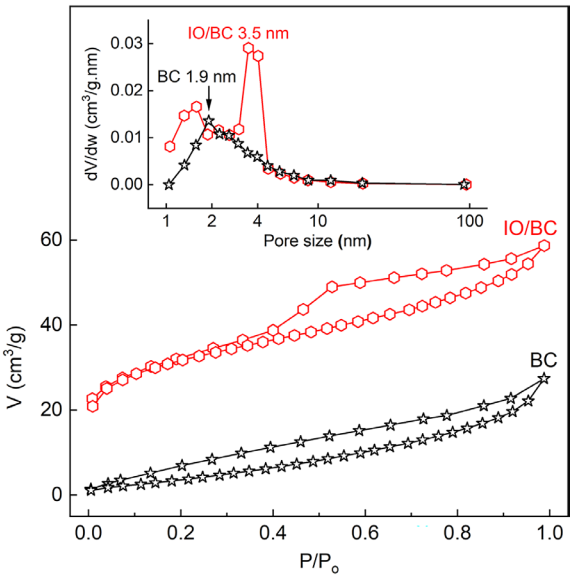

Figure 2. Nitrogen adsorption and desorption isotherms, along with BJH pore size distributions of BC and IO/BC

SEM images of IO/BC are depicted in Figure 3. The material includes microscale fragments with different shapes and sizes. These fragments have rough surfaces and sharp edges. With its soft structure, *C. demersum* was crushed into a fine powder, which might drastically affect the morphology of IO/BC.

Fenton-like degradation of RhB catalyzed by IO/BC

IO/BC was explored as a catalyst for RhB degradation by H_2O_2. BC was also used as a reference sample. All experiments were divided into two steps: initial adsorption lasting 30 min, followed by a 90-min oxidation. The obtained results are shown in Figures 4–8 and Table 2. In general, the adsorption processes reached almost equilibrium within 30 min, and 6–27% RhB was removed. Because only small parts of RhB were removed in the adsorption step, the catalytic performance of IO/BC in the oxidation step could be evaluated accurately.

As presented in Figure 4 and Table 2, the adsorption capacity of IO/BC (3.6 mg/g) exceeded that of BC (2.6 mg/g) in the first step. Compared with BC, IO/BC had higher S_{BET} and V_{total}, possibly resulting in its better adsorption performance. As H_2O_2 was introduced, BC hardly improved RhB removal. Conversely, IO/BC exhibited a high RhB degradation rate. Total RhB removal reached

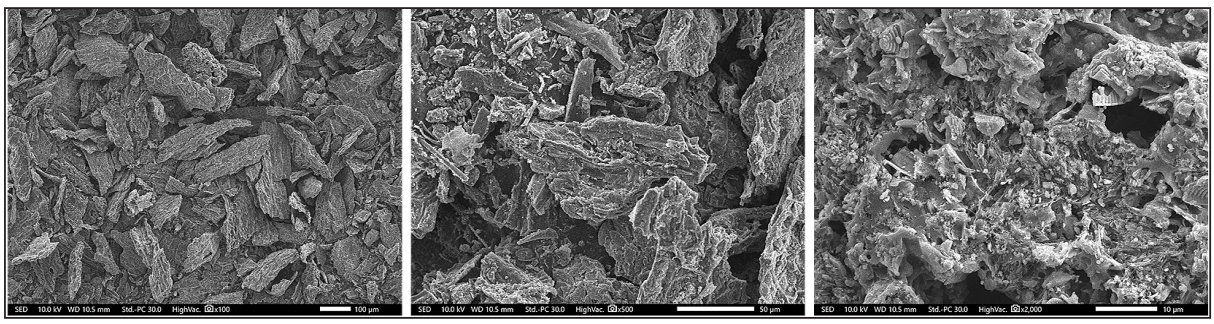

Figure 3. SEM images of IO/BC

92% after 90 min. These results prove that catalytic components mainly come from iron oxides rather than BC. IO/BC contains α-Fe_2O_3 and Fe_3O_4 crystals, which could provide catalytic Fe(II) and Fe(III) sites for the formation of •OH radicals from H_2O_2. According to prior research (Garrido-Ramírez et al., 2010; Thomas et al., 2021), the possible catalytic mechanism is outlined as follows:

$$Fe(II) + H_2O_2 \rightarrow Fe(III) + \bullet OH + OH^- \quad (6)$$

$$Fe(III) + H_2O_2 \rightarrow Fe(II) + H^+ + \bullet OOH \quad (7)$$

$$\bullet OH + RhB \rightarrow \text{Intermediates} \rightarrow CO_2 + H_2O \quad (8)$$

The influence of IO/BC dosage on RhB degradation is depicted in Figure 5. Without IO/BC, H_2O_2 did not directly degrade RhB during 90 min of treatment. In contrast, high RhB degradation rates were observed as different IO/BC dosages were used. These results highlighted the important role of the IO/BC catalyst in RhB degradation with H_2O_2. In addition, increasing IO/BC dosage from 0.25 to 1.00 g/L generally enhanced

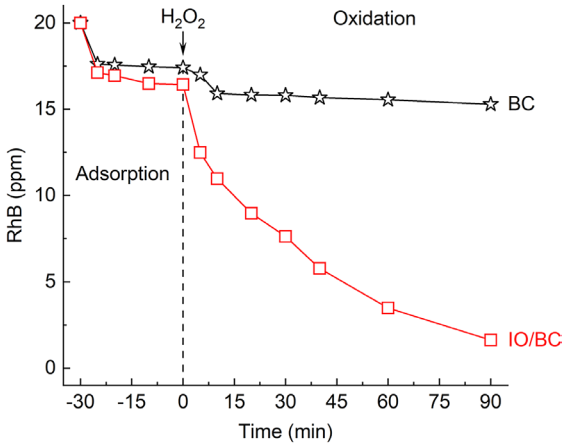

Figure 4. RhB degradation catalyzed by BC and IO/BC (1.00 g/L catalyst, 120 ppm H_2O_2, pH 3.0, 30 °C)

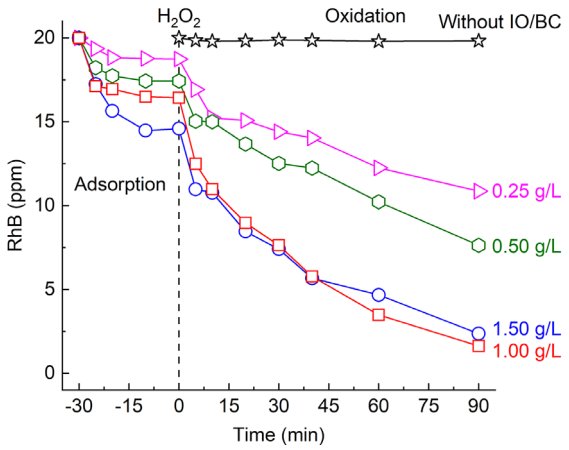

Figure 5. Effect of IO/BC dosage on RhB degradation (120 ppm H_2O_2, pH 3.0, 30 °C)

Table 2. Data summary for RhB removal using H_2O_2 catalyzed by BC and IO/BC

Catalyst	Catalyst dosage (g/L)	pH	H_2O_2 dosage (ppm)	Temperature (°C)	Adsorption (after 30 min)		Oxidation (after 90 min)
					RhB removal (%)	Adsorption capacity (mg/g)	Total RhB removal (%)
BC	1.00	3.0	120	30	13	2.6	24
IO/BC					18	3.6	92
IO/BC	Not used	3.0	120	30	-	-	1
	0.25				6	5.0	46
	0.50				13	5.1	62
	1.00				18	3.6	92
	1.50				27	3.6	88
IO/BC	1.00	2.0	120	30	18	3.6	100
		3.0			18	3.6	92
		4.0			13	2.5	79
		6.0			12	2.3	42
IO/BC	1.00	3.0	Not used	30	19	3.8	19
			60		17	3.4	70
			120		18	3.6	92
			240		15	2.9	90
IO/BC	1.00	3.0	120	20	17	3.4	61
				30	18	3.6	92
				40	12	2.5	99

RhB degradation rate. However, not much difference in RhB degradation rate was recorded between 1.00 and 1.50 g/L IO/BC. Higher IO/BC dosages could offer more catalytic sites for faster RhB degradation. However, an abundance of Fe(II) sites has the potential to deplete •OH radicals (Zhang et al., 2019), as illustrated in the below Equation:

$$Fe(II) + \bullet OH \rightarrow Fe(III) + OH^- \quad (9)$$

pH strongly affected RhB degradation catalyzed by IO/BC (Figure 6). At pH 2.0, RhB degradation occurred rapidly, nearly completely within 40 min of H_2O_2 addition. Despite this, a highly acidic environment may transform iron oxides in IO/BC into aqueous Fe^{2+} and Fe^{3+} ions, deteriorating the stability of IO/BC. When pH increased from 2.0 to 6.0, RhB degradation became slower. In fact, high pH could not only decrease the redox potential of •OH but also promote H_2O_2 decomposition into O_2 rather than •OH (Babuponnusami and Muthukumar, 2014). Additionally, high pH may create Fe(II) and Fe(III)-derived precipitates on the IO/BC surface, reducing the interaction between catalytic sites and species in aqueous media. As a result, pH 3.0 was favorable for Fenton-like processes catalyzed by IO/BC, similar to other iron-based materials (Wang et al., 2016).

Figure 7 illustrates the influence of H_2O_2 dosage on RhB degradation. As previously stated, IO/BC without H_2O_2 only removed a little RhB due to adsorption. When H_2O_2 dosage increased from 60 to 120 ppm, RhB degradation became more rapid. High H_2O_2 dosages could accelerate the formation rate of •OH radicals. However, RhB degradation was not improved by increasing H_2O_2 dosage from 120 to 240 ppm. Excessive H_2O_2 dosage not only causes waste but also eliminates •OH radicals, as described in Equations 10–12 (Nguyen et al., 2021).

$$\bullet OH + H_2O_2 \rightarrow \bullet OOH + H_2O \quad (10)$$

$$\bullet OH + \bullet OOH \rightarrow O_2 + H_2O \quad (11)$$

$$\bullet OH + \bullet OH \rightarrow H_2O_2 \quad (12)$$

As depicted in Figure 8, RhB degradation was boosted as temperature increased from 20 to 40 °C. After 90 min of oxidation, total RhB removals at 20, 30, and 40 °C were 61, 92, and 99%, respectively. High temperatures might enhance electron transfer between IO/BC and H_2O_2 as well as mass transfer. In addition,

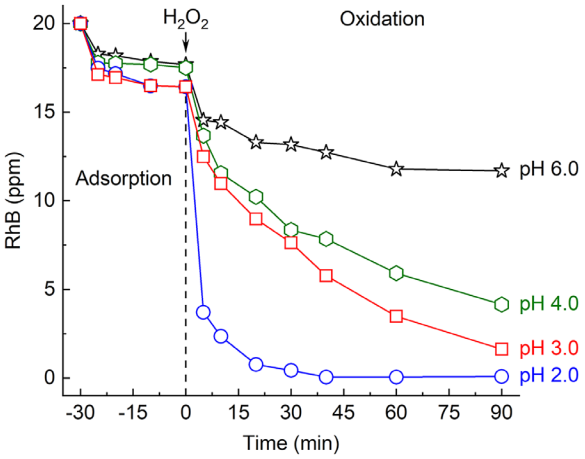

Figure 6. Effect of pH on RhB degradation (1.00 g/L IO/BC, 120 ppm H_2O_2, 30 °C)

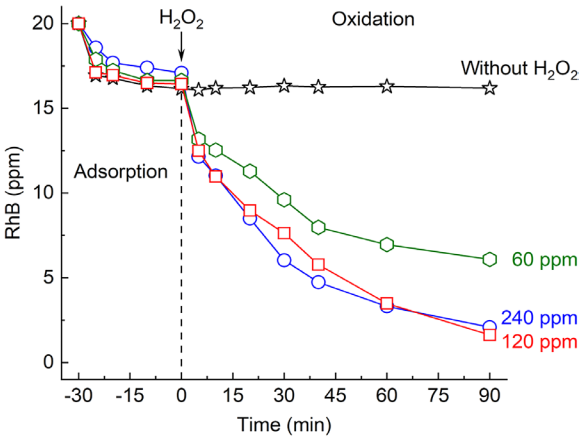

Figure 7. Effect of H_2O_2 dosage on RhB degradation (1.00 g/L IO/BC, pH 3.0, 30 °C)

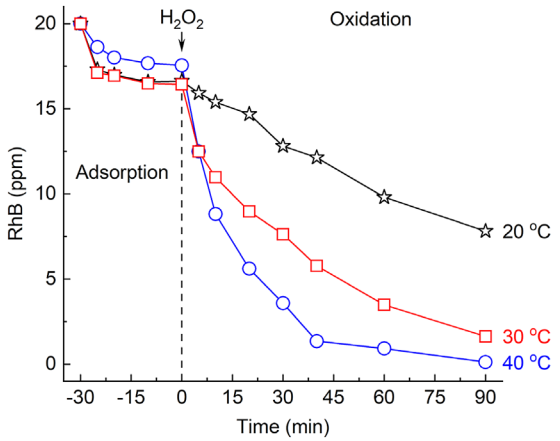

Figure 8. Effect of temperature on RhB degradation (1.00 g/L IO/BC, 120 ppm H_2O_2, pH 3.0)

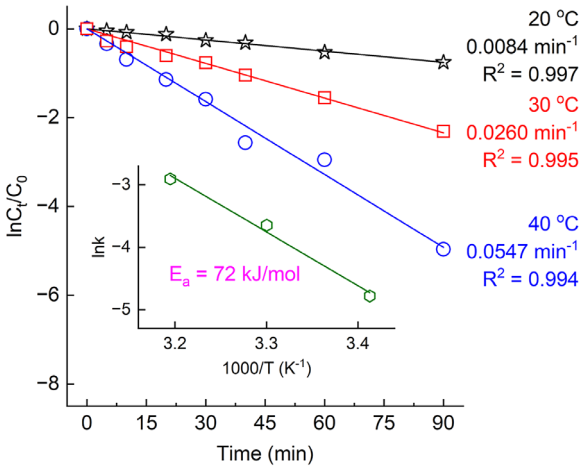

Figure 9. Pseudo-first-order kinetics of RhB degradation at different temperatures and the Arrhenius linear plot

RhB degradation at different temperatures was well fitted with the pseudo-first-order kinetics (Figure 9). Indeed, the degradation rate constants at 20, 30, and 40 °C were 0.0084 (R^2 = 0.997), 0.0260 (R^2 = 0.995), and 0.0547 (R^2 = 0.994) min^{-1}, respectively. Applying the Arrhenius equation, the estimated E_a was 72 kJ/mol, which could be comparable with 82.53 kJ/mol from rice hull-based silica supported iron catalyst (Gan and Li, 2013) or 83.5 kJ/mol from Cu-embedded alumina (Sheng et al., 2018). Thus, IO/BC proved its catalytic potential in activating H_2O_2 for RhB degradation.

CONCLUSIONS

Iron oxide-loaded biochar was prepared successfully from abundant and neglected *C. demersum* and $FeCl_3$ via one-pot pyrolysis. The XRD results showed that the iron oxides formed included α-Fe_2O_3 as the main crystal and Fe_3O_4 as the minor one. Total iron content fixed in IO/BC was 3.19 wt%. Furthermore, IO/BC possessed a V_{total} of 0.091 cm^3/g and a S_{BET} of 113 m^2/g. In the later application, IO/BC removed RhB through adsorption and oxidation manners. In the first step, at pH 3.0, 30 °C, and 1.00 g/L IO/BC, 18% RhB (20 ppm) was eliminated, corresponding to an adsorption capacity of 3.6 mg/g. In the oxidation step, a total of 92% RhB was treated after 90 min of H_2O_2 (120 ppm) addition. In detail, RhB degradation obeyed the pseudo-first-order kinetics and had an estimated E_a of 72 kJ/mol. Altogether, this study not only valorized *C. demersum* but also demonstrated the catalytic potential of low-cost IO/BC for RhB degradation with H_2O_2.

Acknowledgment

This research is funded by Vietnam National University HoChiMinh City (VNU-HCM) under grant number C2024-20-21. We acknowledge Ho Chi Minh City University of Technology (HCMUT), VNU-HCM for supporting this study.

REFERENCES

1. Babuponnusami A. and Muthukumar K. 2014. A review on Fenton and improvements to the Fenton process for wastewater treatment. Journal of Environmental Chemical Engineering, 2(1), 557–572.
2. Bedia J., Peñas-Garzón M., Gómez-Avilés A., Rodriguez J.J. and Belver C. 2020. Review on activated carbons by chemical activation with $FeCl_3$. C, 6(2), 21.
3. Chen J.-Q., Sharifzadeh Z., Bigdeli F., Gholizadeh S., Li Z., Hu M.-L. and Morsali A. 2023. MOF composites as high potential materials for hazardous organic contaminants removal in aqueous environments. Journal of Environmental Chemical Engineering, 11(2), 109469.
4. Do T.V.T., Bui Q.L.N., Nguyen H.M., Lam H.H., Tran-Thuy T.-M., Nguyen L.Q., Ngo D.T.H. and Nguyen D.V. 2022. One-pot fabrication of magnetic biochar by $FeCl_3$-activation of lotus seedpod and its catalytic activity towards degradation of Orange G. Materials Research Express, 9(10), 105601.
5. Feng Z., Yuan R., Wang F., Chen Z., Zhou B. and Chen H. 2021. Preparation of magnetic biochar and its application in catalytic degradation of organic pollutants: A review. Science of The Total Environment, 765, 142673.
6. Filote C., Roșca M., Hlihor R.M., Cozma P., Simion I.M., Apostol M. and Gavrilescu M. 2021. Sustainable application of biosorption and bioaccumulation of persistent pollutants in wastewater treatment: Current practice. Processes, 9(10), 1696.
7. Gan P.P. and Li S.F.Y. 2013. Efficient removal of Rhodamine B using a rice hull-based silica supported iron catalyst by Fenton-like process. Chemical Engineering Journal, 229, 351–363.
8. Garrido-Ramírez E.G., Theng B.K.G. and Mora M.L. 2010. Clays and oxide minerals as catalysts and nanocatalysts in Fenton-like reactions — A review. Applied Clay Science, 47(3), 182–192.
9. Ghibate R., Kerrou M., Chrachmy M., Baaziz M.B., Taouil R. and Senhaji O. 2024. Utilizing agricultural

waste for sustainable remediation of textile dyeing effluents. Ecological Engineering & Environmental Technology, 25(7), 369–378.

10. Gupta M., Savla N., Pandit C., Pandit S., Gupta P.K., Pant M., Khilari S., Kumar Y., Agarwal D., Nair R. R., Thomas D. and Thakur V.K. 2022. Use of biomass-derived biochar in wastewater treatment and power production: A promising solution for a sustainable environment. Science of The Total Environment, 825, 153892.
11. Gutiérrez L., de la Cueva L., Moros M., Mazarío E., de Bernardo S., de la Fuente J. M., Morales M. P. and Salas G. 2019. Aggregation effects on the magnetic properties of iron oxide colloids. Nanotechnology, 30(11), 112001.
12. Keskinkan O., Goksu M.Z.L., Basibuyuk M. and Forster C. F. 2004. Heavy metal adsorption properties of a submerged aquatic plant (*Ceratophyllum demersum*). Bioresource Technology, 92(2), 197–200.
13. Liu Y. and Wang J. 2023. Multivalent metal catalysts in Fenton/Fenton-like oxidation system: A critical review. Chemical Engineering Journal, 466, 143147.
14. Lu F. and Astruc D. 2020. Nanocatalysts and other nanomaterials for water remediation from organic pollutants. Coordination Chemistry Reviews, 408, 213180.
15. Masud M.A.A., Shin W.S., Sarker A., Septian A., Das K., Deepo D.M., Iqbal M.A., Islam A.R.M.T. and Malafaia G. 2023. A critical review of sustainable application of biochar for green remediation: Research uncertainty and future directions. Science of The Total Environment, 904, 166813.
16. Mokrzycki J., Michalak I. and Rutkowski P. 2021. Biochars obtained from freshwater biomass—green macroalga and hornwort as Cr(III) ions sorbents. Biomass Conversion and Biorefinery, 11(2), 301–313.
17. Mukhopadhyay A., Duttagupta S. and Mukherjee A. 2022. Emerging organic contaminants in global community drinking water sources and supply: A review of occurrence, processes and remediation. Journal of Environmental Chemical Engineering, 10(3), 107560.
18. Nguyen H.M., Nguyen L.T., Nguyen L.T.K., Lam H.H., Tran-Thuy T.-M., Nguyen L.Q. and Nguyen D.V. 2021. Facile preparation of lotus seedpod-derived magnetic porous carbon for catalytic oxidation of Ponceau 4R. IOP Conference Series: Earth and Environmental Science, 947(1), 012019.
19. Nguyen H.M., Truong T.B., Nguyen H.-H.T., Tran P.T., Tran-Thuy T.-M., Nguyen L.Q. and Nguyen D.V. 2023. Catalytic ozonation of Ponceau 4R using multifunctional magnetic biochar prepared from rubber seed shell. Journal of Ecological Engineering, 24(12), 143–151.
20. Nguyen N.T.K., Le D.T.T., Vo K.D., Huynh L.T., Nguyen H.M., Tran-Thuy T.-M., Nguyen L.Q. and Nguyen D.V. 2024. Valorization of tropical almond (*Terminalia catappa*) leaves into iron-containing activated carbon for rapid catalytic degradation of methylene blue with hydrogen peroxide. Journal of Ecological Engineering, 25(8), 54-61.
21. Novia N., Agustina T.E., Riduan S. and Pangestu G. 2023. Testing of a laboratory wastewater treatment prototype using coagulation, adsorption and photo-Fenton processes. Ecological Engineering & Environmental Technology, 24(5), 202–209.
22. Pereira Lopes R. and Astruc D. 2021. Biochar as a support for nanocatalysts and other reagents: Recent advances and applications. Coordination Chemistry Reviews, 426, 213585.
23. Polechońska L., Klink A., Dambiec M. and Rudecki A. 2018. Evaluation of *Ceratophyllum demersum* as the accumulative bioindicator for trace metals. Ecological Indicators, 93, 274–281.
24. Qadri H., Uqab B., Javeed O., Dar G.H. and Bhat R.A. 2022. *Ceratophyllum demersum*-An accretion biotool for heavy metal remediation. Science of The Total Environment, 806, 150548.
25. Qin F., Zhang C., Zeng G., Huang D., Tan X. and Duan A. 2022. Lignocellulosic biomass carbonization for biochar production and characterization of biochar reactivity. Renewable and Sustainable Energy Reviews, 157, 112056.
26. Qu J., Shi J., Wang Y., Tong H., Zhu Y., Xu L., Wang Y., Zhang B., Tao Y., Dai X., Zhang H. and Zhang Y. 2022. Applications of functionalized magnetic biochar in environmental remediation: A review. Journal of Hazardous Materials, 434, 128841.
27. Rahim Pouran S., Abdul Raman A.A. and Wan Daud W.M.A. 2014. Review on the application of modified iron oxides as heterogeneous catalysts in Fenton reactions. Journal of Cleaner Production, 64, 24–35.
28. Rusevova K., Kopinke F.-D. and Georgi A. 2012. Nano-sized magnetic iron oxides as catalysts for heterogeneous Fenton-like reactions—Influence of Fe(II)/Fe(III) ratio on catalytic performance. Journal of Hazardous Materials, 241–242, 433–440.
29. Sheng Y., Sun Y., Xu J., Zhang J. and Han Y.-F. 2018. Fenton-like degradation of rhodamine B over highly durable Cu-embedded alumina: Kinetics and mechanism. AIChE Journal, 64(2), 538–549.
30. Shokri A. and Fard M.S. 2022. A critical review in Fenton-like approach for the removal of pollutants in the aqueous environment. Environmental Challenges, 7, 100534.
31. Thomas N., Dionysiou D.D. and Pillai S.C. 2021. Heterogeneous Fenton catalysts: A review of recent advances. Journal of Hazardous Materials, 404, 124082.
32. Titchou F.E., Zazou H., Afanga H., El Gaayda J., Ait Akbour R., Nidheesh P.V. and Hamdani M. 2021.

Removal of organic pollutants from wastewater by advanced oxidation processes and its combination with membrane processes. Chemical Engineering and Processing - Process Intensification, 169, 108631.

33. Wang D., Gan X., Wang Z., Jiang S., Zheng X., Zhao M., Zhang Y., Fan C., Wu S. and Du L. 2023. Research status on remediation of eutrophic water by submerged macrophytes: A review. Process Safety and Environmental Protection, 169, 671–684.
34. Wang N., Zheng T., Zhang G. and Wang P. 2016. A review on Fenton-like processes for organic wastewater treatment. Journal of Environmental Chemical Engineering, 4(1), 762–787.
35. Weidner E., Karbassiyazdi E., Altaee A., Jesionowski T. and Ciesielczyk F. 2022. Hybrid metal oxide/biochar materials for wastewater treatment technology: A review. ACS Omega, 7(31), 27062–27078.
36. Yi Y., Huang Z., Lu B., Xian J., Tsang E. P., Cheng W., Fang J. and Fang Z. 2020. Magnetic biochar for environmental remediation: A review. Bioresource Technology, 298, 122468.
37. Zeng S. and Kan E. 2022. $FeCl_3$-activated biochar catalyst for heterogeneous Fenton oxidation of antibiotic sulfamethoxazole in water. Chemosphere, 306, 135554.
38. Zhang M.-h., Dong H., Zhao L., Wang D.-x. and Meng D. 2019. A review on Fenton process for organic wastewater treatment based on optimization perspective. Science of The Total Environment, 670, 110–121.
39. Zhao C., Wang B., Theng B.K.G., Wu P., Liu F., Wang S., Lee X., Chen M., Li L. and Zhang X. 2021. Formation and mechanisms of nano-metal oxide-biochar composites for pollutants removal: A review. Science of The Total Environment, 767, 145305.
40. Zhu Y., Zhu R., Xi Y., Zhu J., Zhu G. and He H. 2019. Strategies for enhancing the heterogeneous Fenton catalytic reactivity: A review. Applied Catalysis B: Environmental, 255, 117739.